Synthesis of Ce:YIG nanopowder by gel combustion

M. N. Smirnova[1], I. S. Glazkova[2], G. E. Nikiforova[1], M. A. Kop'eva[1], A. A. Eliseev[2],
E. A. Gorbachev[2], V. A. Ketsko[1]

[1]Kurnakov Institute of General and Inorganic Chemistry of the Russian Academy of Sciences,
119991, 31 Leninsky Prospect, Moscow, Russia
[2]Department of Chemistry, Lomonosov Moscow State University 119234, 1 Leninskie Gory, Moscow, Russia

smirnovamn@igic.ras.ru, janglaz@bk.ru, gen@igic.ras.ru, mkopieva@mail.ru, artem.a.eliseev@gmail.com,
gorbach.ev.genij@gmail.com, ketsko@igic.ras.ru

Nanocrystalline Ce-substituted yttrium iron-gallium garnet $Y_{2.5}Ce_{0.5}(Fe_{0.5}Ga_{0.5})_5O_{12}$ was obtained by a metal-organic gel combustion method using PVA as a fuel with subsequent calcining in vacuum at 700 $^\circ$C. According to SEM and XRD data, an additional heat treatment in air led only to an increase in the crystallinity of the sample. The element composition and the phase purity were confirmed by X-ray fluorescence spectroscopy and X-ray powder diffraction, respectively. Mössbauer spectroscopy on ^{57}Fe nuclei revealed the presence of only Fe^{3+} ions in the sample, which can be considered as indirect evidence of the absence of tetravalent cerium impurity.

Keywords: gel combustion, ferrites, cerium yttrium iron garnet, nanoparticles.

Received: 21 January 2021

Revised: 22 March 2021

1. Introduction

For a number of years, ferrite-garnets have been the subject of numerous studies [1–7]. Interest in this class of compounds is due to their unique magnetic and magneto-optical properties [1–3]. The presence in the crystal lattice of three different crystallographic positions (dodecahedral, tetrahedral, octahedral) and the tendency of garnets to undergo isomorphic substitution allows changing their physicochemical and functional characteristics within wide limits [3].

One of the most well known ferrite garnets is yttrium iron garnet (YIG) – $Y_3Fe_5O_{12}$, which is used in microwave technology because of the extremely narrow ferromagnetic resonance absorption line [2]. According to theoretical estimates, replacing Y^{3+} in YIG with Ce^{3+} enhances magneto-optical activity in the visible and near infrared ranges [4–8], reduces optical power losses (attenuation of the light signal) [8], and helps to lower the crystallization temperature of garnet. These factors expand the possible areas of application of materials based on YIG for the creation of new generation magneto-optical devices [3–5].

However, the possibility of replacing Y^{3+} with Ce^{3+} in garnet has structural limitations. Since the effective ionic radius of Ce^{3+} (1.14 Å) is larger than the radius of yttrium Y^{3+} (1.02 Å) [9], with an increase in the cerium concentration, internal stresses and structural distortions of the crystal are induced [10]. This problem can be solved by the introduction of smaller ions (for example, Al^{3+} or Ga^{3+} cations) into YIG together with Ce^{3+}, which makes it possible to compensate for structural limitations and promotes the formation of garnet of a given composition [11–14]. The literature contains data on the preparation of Ce:YIG ceramics without replacing Fe^{3+} with other cations, but in these studies, the cerium content in garnet did not exceed 8 %, for example, $Ce_{0.122}Y_{2.878}Fe_5O_{12}$ [5], $Ce_{0.15}Y_{2.85}Fe_5O_{12}$ [14], $Ce_{0.25}Y_{2.75}Fe_5O_{12}$ [4].

Another factor limiting the solubility of cerium in YIG is the tendency of Ce^{3+} to oxidize and transform into a diamagnetic tetravalent state. Huang et al. [5] considered the possibility of increasing the concentration of Ce^{3+} ions in the YIG structure and "suppressing" the formation of nonmagnetic Ce^{4+} ions by means of charge compensation due to the introduction of Eu^{3+} ions into the dodecahedral yttrium positions. Nevertheless, the maximum possible content of Ce^{3+} in this case did not exceed 12 %, $Ce_{0.349}Eu_{0.195}Y_{2.456}Fe_5O_{12}$.

Another significant problem is the necessity of using high processing temperatures in the synthesis of polycrystalline Ce-substituted garnets by the solid-state reactions [4–6]. High-temperature annealing in an oxidizing atmosphere inevitably leads to partial oxidation of Ce^{3+} and the formation of a stable CeO_2 impurity that does not possess magnetic ordering, which impairs the magnetic and magneto-optical properties of YIG.

Previously, Opuchovic et al. [15] tried to solve the problem of CeO_2 formation by annealing the precursor obtained during the synthesis of $Y_{3-x}Ce_xFe_5O_{12}$ by the sol-gel method in a reducing atmosphere of CO. However, this treatment prevented not only the formation of CeO_2, but also the formation of the garnet itself. The main phase for all

compositions was perovskite. In the Y–Fe–O system, the perovskite structure is energetically more favorable and is formed at lower temperatures [16]. On the contrary, in the yttrium-gallium oxide system, the preparation of perovskite is extremely difficult [17]. Thus, the partial substitution of gallium for iron ions, which allows stabilizing the garnet structure, together with the use of an oxygen-deficient calcination atmosphere, may be promising for the production of Ce:YIG with a higher degree of substitution.

In this regard, our studies were aimed at studying $Y_{3-x}Ce_x(Fe_{1-y}Ga_6)_5O_{12}$ solid solutions in order to obtain a composition with the highest possible substitution of Ce^{3+} for Y^{3+} in the absence of tetravalent cerium impurities in the resulting garnet.

For the synthesis of the samples, the method of the gel combustion was chosen [12, 13], the advantages of which are largely associated with the short duration of the high-temperature stage of decomposition of the gel-like precursor, which contributes to the relatively rapid formation of the crystalline phase, hinders the formation of undesirable impurities and makes it possible to obtain nanosized polycrystalline powder materials [17–21]. Nitrates of the yttrium, cerium, iron, gallium and polyvinyl alcohol (PVA) were used as starting reagents for the preparation of $Y_{3-x}Ce_x(Fe_{1-y}Ga_y)_5O_{12}$ garnets. The efficiency of PVA application for the synthesis of cation-substituted garnets by gel combustion was shown earlier [12, 20, 22]. Due to the hydrophilic OH groups, polyvinyl alcohol ensures the complexation process, which contributes to the uniform distribution of hydrated metal cations in the gel structure, prevents segregation and the formation of undesirable individual oxide compounds during solution evaporation.

Particular attention was paid to the creation of oxygen-deficient conditions during heat treatment of the samples to reduce the probability of the oxidation of Ce^{3+} ions to Ce^{4+}. In this regard, the calcination of the samples immediately after synthesis was carried out in vacuum.

2. Experimental

2.1. Synthesis procedure

Aqueous solutions of yttrium, cerium, iron and gallium nitrates were prepared separately for each sample by dissolving stoichiometric amounts of yttrium carbonate trihydrate ($Y_2(CO_3)_3 \cdot 3H_2O$, > 99.9 %), cerium nitrate hexahydrate ($Ce(NO_3)_3 \cdot 6H_2O$, > 99.8 %), carbonyl iron powder (Fe, > 99.99 %) and metallic gallium (Ga, > 99.99 %) in dilute nitric acid. Polyvinyl alcohol (PVA) was added to the resulting solution at the ratio of 0.12 mol of $(CH_2CHOH)_n$ per 0.01 mol of garnet.

The reaction mixtures were evaporated in porcelain bowls on a hotplate with constant stirring until gels were formed. With a further increase in temperature to 100 °C, the gels burned and turned into fine powders, the color of which varied from yellow-beige to brown. After cooling, the powders were dispersed with a ball mill and annealed at 700 °C in an oven for 2 hours at a pressure of about 10^{-2} Pa.

2.2. Characterization of the samples

X-ray powder diffraction (XRD) was performed using a Bruker D8 Advance diffractometer equipped with Ni-filtered (CuK$_{\alpha 1}$-radiation) and a LYNXEYE detector in the angle range $2\theta = 10° - 70°$ with a scanning step of $0.0133°$ and a counting time of 0.3 s per step. The results of XRD experiments were interpreted using the Bruker DIFFRAC.EVA software package and the ICDD PDF-2 database.

The chemical composition of the samples was determined using a Bruker M4 TORNADO μ-X-ray fluorescence spectrometer equipped with a Rh-anode X-ray tube with a polycapillary lens. The accuracy of μ-XRF analysis was ± 5 %.

The surface morphology and microstructure of $Y_{3-x}Ce_x(Fe_{1-y}Ga_y)_5O_{12}$ were investigated using a Carl Zeiss NVision 40 scanning electron microscope (SEM). SEM micrographs were obtained with an Everhart–Thornley secondary electron (SE2) detector.

The specific surface area of sample obtained was measured by the low-temperature nitrogen adsorption method using a Katakon ATKh-O6 analyzer. Before measurements, the sample was degassed in a nitrogen flow at 200 °C for 60 min. The specific surface area of the sample S_{BET} was calculated using the Brunauer–Emmett–Teller (BET) model at 5 points in the range of partial pressures of $0.05 - 0.25$ P/P_0.

^{57}Fe Mössbauer spectra were measured using a conventional constant-acceleration MS-110Em spectrometer. To analyze the Mössbauer data, we used the methods of model interpretation and reconstruction of the distribution of hyperfine parameters, implemented in the SpectrRelax software [23]. Isomer shifts of the ^{57}Fe Mössbauer spectra are given relative to α-Fe at 298 K.

3. Results and discussion

The effect of oxygen-deficient heat treatment conditions on the formation of the garnet structure was studied on the samples of the $Y_{2.8}Ce_{0.2}Fe_{5-y}Ga_yO_{12}$ solid solution with different contents of iron and gallium, synthesized by the gel combustion method followed by annealing in vacuo at 700 °C. The X-ray diffraction patterns (Fig. 1) show that in the absence of gallium dopant ($y = 0$), both garnet and perovskite crystalline phases are formed in almost equal amounts. In this case, cerium atoms were not incorporated into any of the structures, but formed a cubic solid solution based on yttrium oxide $(Y,Ce)_2O_{3+\delta}$. When a small amount of gallium ($y = 1$) was added to the composition, the crystalline phase of garnet became the main one. However, the X-ray diffraction patterns retained a small number of additional reflections, which completely disappeared only for the composition with $y = 2.5$.
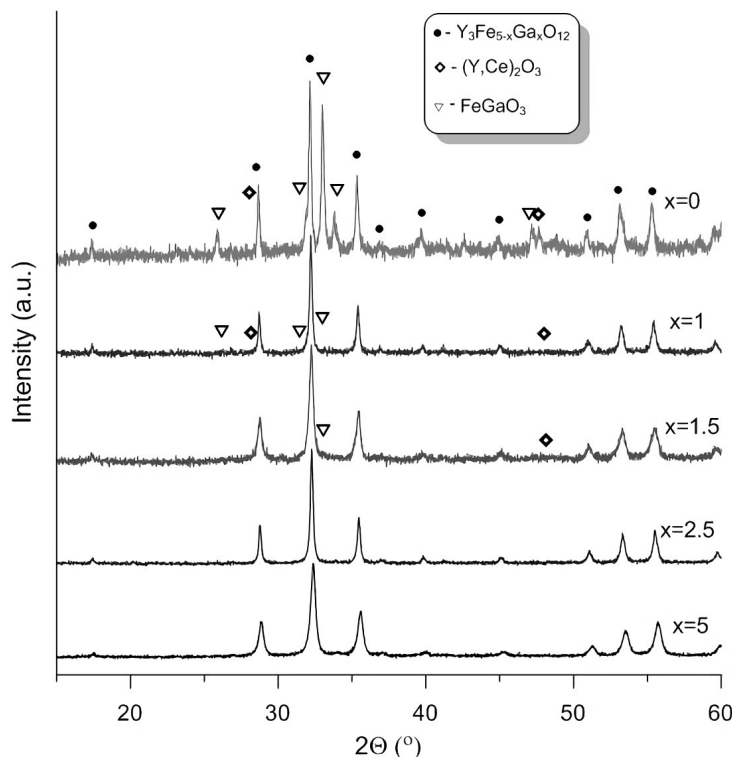

FIG. 1. XRD patterns of $Y_{2.8}Ce_{0.2}Fe_{5-y}Ga_yO_{12}$ powders prepared by vacuum heat treatment at 700 °C for 2 h

Thus, the results of this experiment allow us to conclude that, when Fe^{3+} ions are replaced by Ga^{3+}, the garnet structure is more stable than perovskite not only in air, but also in an oxygen-deficient atmosphere. In addition, the presence of Ga^{3+} ions compensates for the crystal stresses in the garnet structure arising from the substitution of Ce^{3+} for Y^{3+}. To further study the incorporation of cerium ions into the garnet structure, a composition with 50 % substitution of gallium for iron was chosen.

The X-ray powder diffraction of Ce-substituted garnets $Y_{3-x}Ce_x(Fe_{0.5}Ga_{0.5})_5O_{12}$ annealed in vacuum at 700 °C (Fig. 2) showed that, with the partial substitution of cerium for yttrium, the homogeneity of the garnet phase was retained only up to the cerium content $x = 0.5$. A further increase in the amount of cerium in the nominal composition of the samples led to the appearance of diffuse reflections in the XRD patterns, which could be attributed to the formation of a cerium dioxide impurity. The incorporation of cerium ions into the garnet structure and the formation of a solid solution could be confirmed by a monotonic change in the crystal lattice parameter a from 12.346(2) to 12.397(1) Å as the cerium content increased to $x = 0.5$.

The ratio of cations in the $Y_{2.5}Ce_{0.5}(Fe_{0.5}Ga_{0.5})_5O_{12}$ sample was confirmed by X-ray fluorescence analysis and energy-dispersive X-ray spectroscopy. Both methods showed that the composition of the studied sample was close to the theoretical one within the experimental error (Fig. 3, Table 1).

Figure 4 shows SEM images of $Y_{2.5}Ce_{0.5}(Fe_{0.5}Ga_{0.5})_5O_{12}$ garnet obtained in an oxygen-deficient atmosphere. After vacuum heat treatment, the sample consists of tightly "pressed" large agglomerates, forming almost monolithic plates. At the fracture site, these agglomerates of indefinite shape have a porous spongy structure. With such sample
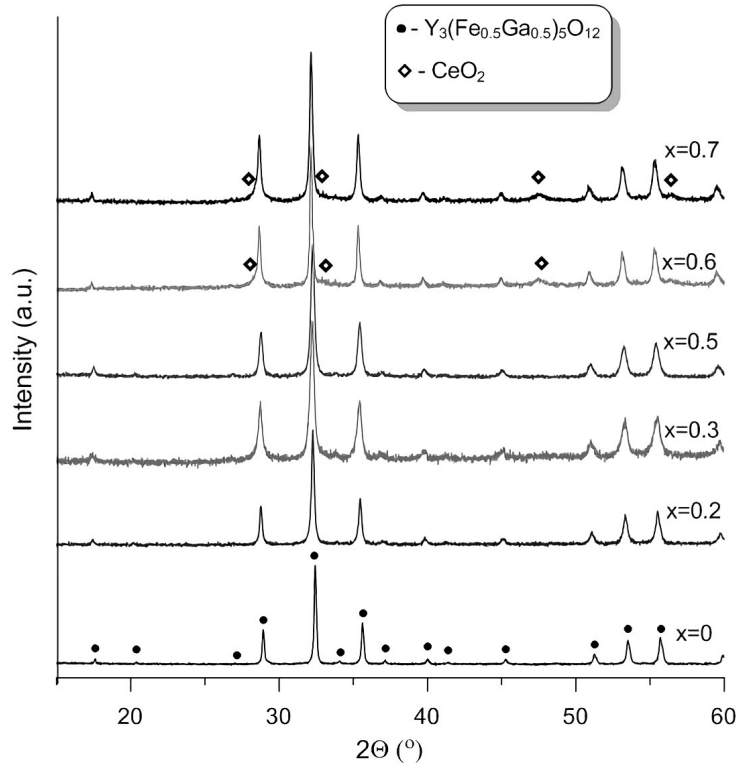
FIG. 2. XRD patterns of $Y_{3-x}Ce_x(Fe_{0.5}Ga_{0.5})_5O_{12}$ powders prepared by vacuum heat treatment at 700 °C for 2 h
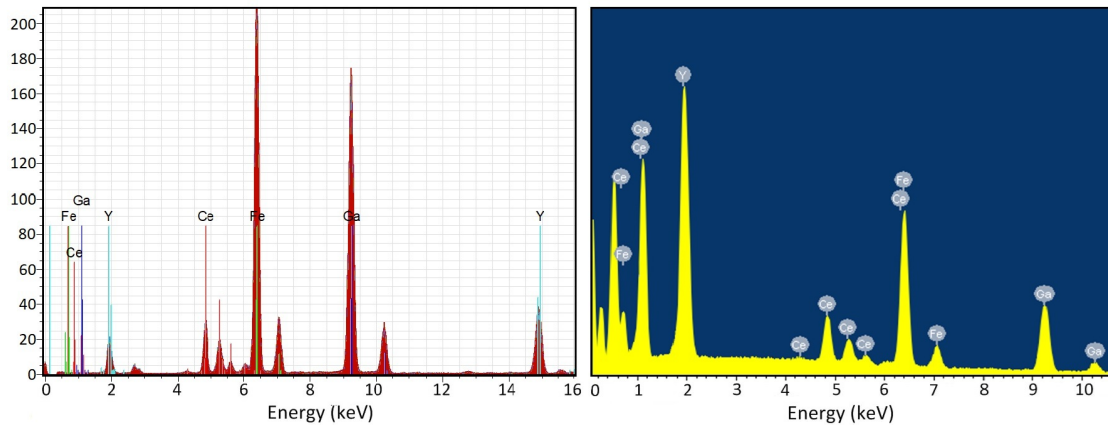

FIG. 3. μ-XRF and EDS spectra of $Y_{2.5}Ce_{0.5}(Fe_{0.5}Ga_{0.5})_5O_{12}$ nanopowder

morphology, there is a possibility that some of the Ce^{3+} ions are not incorporated into the garnet structure and are present in the sample as an amorphous impurity. Additional annealing in air at a higher temperature should promote the oxidation of unbound cerium and its transition to the tetravalent state.

After heat treatment in vacuum, the $Y_{2.5}Ce_{0.5}(Fe_{0.5}Ga_{0.5})_5O_{12}$ sample was additionally calcined in air at 800 °C for 5 hours. SEM images (Fig. 5) show that the surface of the plates did not change, however, the morphology of the sample underwent significant changes on the spalls. Each plate consists of small monodisperse randomly located particles, 70 – 80 nm in size, forming a porous structure resembling an openwork fabric. This morphology of the sample is associated with the use of the gel combustion method for its preparation. The main stage of this process is the combustion of the organometallic gel, accompanied by the removal of gaseous pyrolysis products, which contributes to the dispersion of the precursor and the formation of a highly dispersed final powder.

TABLE 1. Results of μ-XRF and EDS studies of $Y_{2.5}Ce_{0.5}(Fe_{0.5}Ga_{0.5})_5O_{12}$ nanopowder

Element	wt. %		
	Theoretical value	Observed value	
		μ-XRF	EDS
Y	36.66	36.41	36.46
Ce	11.56	11.43	11.78
Fe	23.03	23.23	22.94
Ga	28.75	28.93	28.82
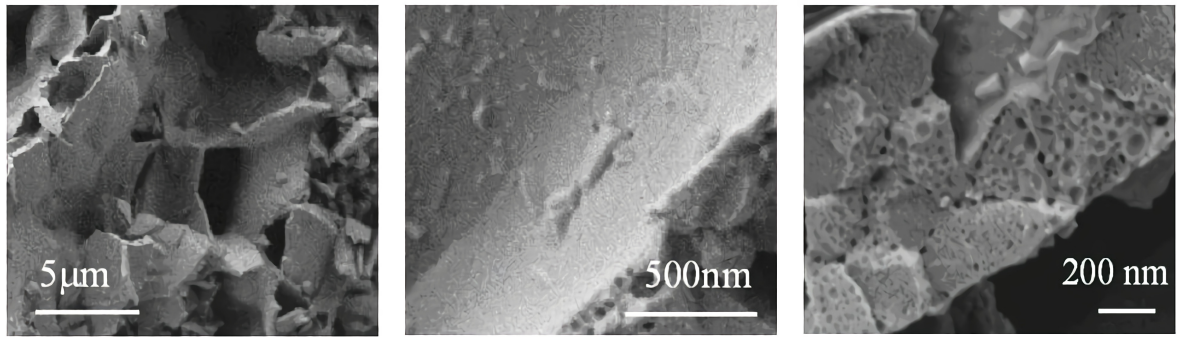
FIG. 4. SEM images of $Y_{2.5}Ce_{0.5}(Fe_{0.5}Ga_{0.5})_5O_{12}$ nanopowder after vacuum heat treatment at 700 °C, obtained at different magnifications
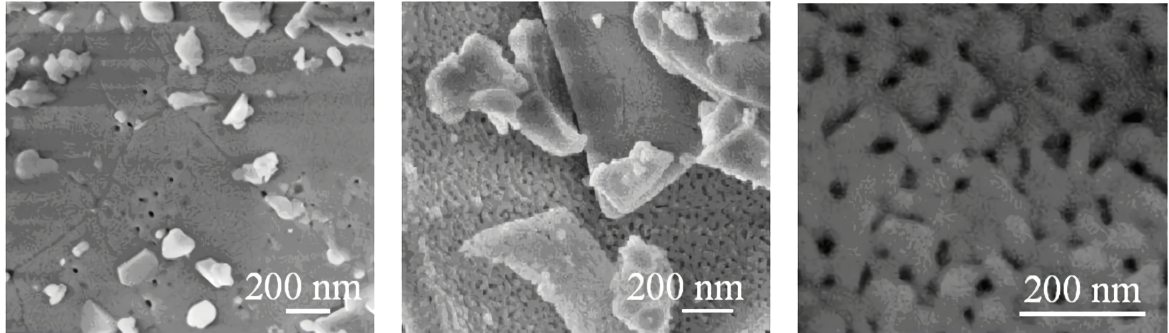
FIG. 5. SEM images of $Y_{2.5}Ce_{0.5}(Fe_{0.5}Ga_{0.5})_5O_{12}$ nanopowder after annealing in air at 800 °C, obtained at different magnifications

According to X-ray diffraction data, the sample after annealing in air remained single-phase; no reflections of impurity phases were recorded. The results of a full-profile analysis of the XRD data of the $Y_{2.5}Ce_{0.5}(Fe_{0.5}Ga_{0.5})_5O_{12}$ powder additionally annealed in air at 800 °C are shown in Fig. 6. The sample has a cubic garnet structure ($Ia - 3d$) with the parameters: $a = 12.397$ Å, $V = 1905.2$ Å^3.

The size of the coherent scattering domains, taken as the average particle size, was calculated using the Scherrer equation and amounted to 67 nm. This value, calculated from the broadening of the X-ray lines, agrees very well with the particle size observed by SEM.

The specific surface area (S_{BET}) of the $Y_{2.5}Ce_{0.5}(Fe_{0.5}Ga_{0.5})_5O_{12}$ nanopowder calculated using the multipoint BET-equation was 9.3 m^2/g. Since the sample consists of monodisperse isotropic particles, the average particle size D_{BET} (nm) can be calculated using the equation:
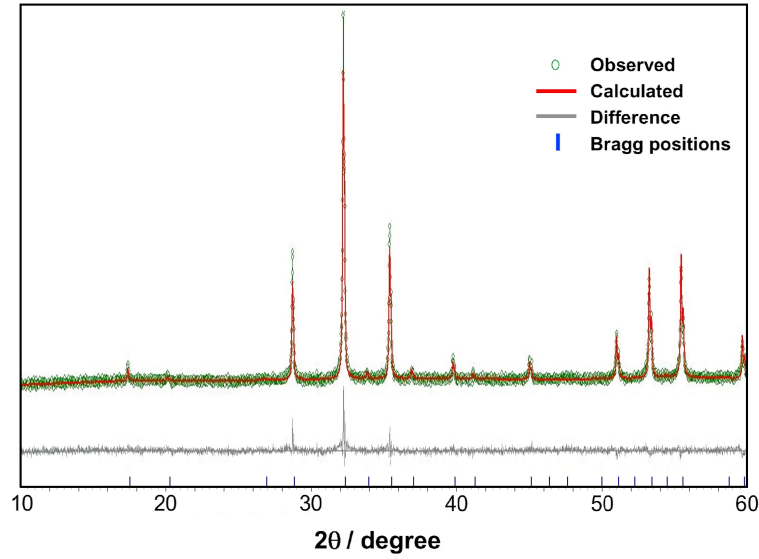
$$D_{BET} = 6000/(\rho_{cr} \cdot S_{BET}),$$

FIG. 6. The Pawley refinement plot of the XRD data for the $Y_{2.5}Ce_{0.5}(Fe_{0.5}Ga_{0.5})_5O_{12}$ nanopowder

where ρ_{cr} is a crystallographic density (5.57 g/cm^3).

The average particle size calculated from BET analysis was 115 nm. This value is greater than the above-mentioned particle sizes determined from the results of SEM and X-ray diffraction. The reason for this may be that some nanoparticles are agglomerated into plates (Fig. 5), which led to an overestimation of the D_{BET} value.

When cerium is incorporated into the garnet structure, cation-cation interactions between octahedral crystallographic positions, in which iron and gallium atoms are located, and dodecahedral crystallographic positions, in which yttrium and cerium atoms are located, are enhanced [24, 25]. This can lead to a redistribution of charges within the crystal structure and a change in the valence state of iron and cerium.

The ^{57}Fe Mössbauer spectra of the $Y_3(Fe_{0.5}Ga_{0.5})_5O_{12}$ and $Y_{2.5}Ce_{0.5}(Fe_{0.5}Ga_{0.5})_5O_{12}$ garnets measured at room temperature represent a complex superposition of two asymmetrically broadened quadrupole doublets (Fig. 7a).

Both spectra resemble those of unsubstituted garnets [26–28] and do not contain magnetically-split components, which confirms the absence of impurity phases like perovskite- or spinel-type ferrites. At the same time, the replacement of some of the iron cations with gallium cations and the replacement of Y^{3+} with Ce^{3+} leads to a significant broadening of the resonance lines. Therefore, the fitting procedure of the spectra was performed by the reconstruction of the distribution of quadrupole doublets taking into account the linear correlation of shifts δ and quadrupole splitting Δ (Fig. 7b). The obtained values of the hyperfine parameters of the spectra (Table 2) show that the iron cations in both garnets are stabilized only in 3+ oxidation state in two nonequivalent sites. This experimental fact indirectly indicates that in the structure of $Y_{2.5}Ce_{0.5}(Fe_{0.5}Ga_{0.5})_5O_{12}$, as a result of the replacement of some of the yttrium atoms with cerium atoms, the latter are not oxidized. It should be noted that the obtained ratio of iron cations in tetrahedral and octahedral positions calculated from the relative partial spectra (I) deviates somewhat from 3:2 ratio given by the structure (Table 2), which indicates a greater preference for gallium atoms in the structures of these garnets for tetrahedral oxygen positions.

4. Conclusions

Here, we present the results of the synthesis and study of a solid solution of cerium-substituted yttrium iron garnet aimed at achieving the maximum possible substitution of Y^{3+} with Ce^{3+}. The replacement of Fe^{3+} ions by Ga^{3+} in a 1:1 ratio and the use of vacuum annealing of the precursor obtained by gel combustion method made it possible to increase cerium content in the garnet structure to 16.7 % relative to yttrium and avoid the formation of CeO_2 impurities.

The study of the $Y_{2.5}Ce_{0.5}Fe_{2.5}Ga_{2.5}O_{12}$ nanopowder by ^{57}Fe Mössbauer spectroscopy showed the presence of iron cations in the structure only in 3+ formal oxidation state, which is an additional confirmation of the phase homogeneity of this composition, as well as indirect evidence of the absence of both CeO_2 impurities and Ce^{4+} ions in the $Y_{2.5}Ce_{0.5}(Fe_{0.5}Ga_{0.5})_5O_{12}$ structure.
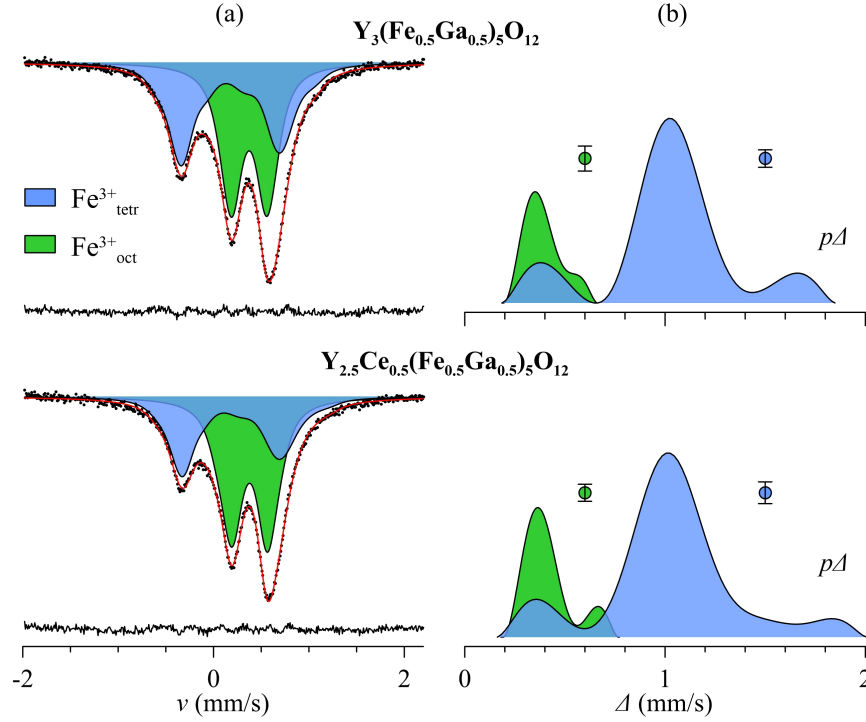
FIG. 7. (a) The ^{57}Fe Mössbauer spectra of $Y_{3-x}Ce_x(Fe_{0.5}Ga_{0.5})_5O_{12}$ ($x = 0, 0.5$) nanopowders measured at $T = 298$ K; (b) the corresponding distributions of the quadrupole splittings $p\Delta$

TABLE 2. The hyperfine parameters of the ^{57}Fe Mössbauer spectra of $Y_{3-x}Ce_x(Fe_{0.5}Ga_{0.5})_5O_{12}$ ($x = 0, 0.5$) nanopowders at $T = 298$ K

Cerium content x	Partial spectrum	δ^* (mm/s)	Δ^* (mm/s)	I (%)
0	Fe^{3+}_{tetr}	0.18(1)	1.02(1)	47.6(5)
	Fe^{3+}_{oct}	0.37(1)	0.39(1)	52.4(5)
0.5	Fe^{3+}_{tetr}	0.18(1)	1.02(1)	40.0(5)
	Fe^{3+}_{oct}	0.38(1)	0.41(1)	60.0(5)

δ – isomer shift; Δ – quadrupole splitting;

I – relative intensity of the corresponding partial spectrum;

$*$ – the mean values of the mean values of δ and Δ was estimated from

the distributions $p\delta$ and $p\Delta$.

Thus, low-temperature heat treatment of the samples under vacuum conditions prevents the oxidation of Ce^{3+} to Ce^{4+} and minimizes the probability of CeO_2 formation.

The synthesized nanocrystalline Ce:YIG powder has a developed surface and a monodisperse porous structure, which makes it promising for industrial and technical applications. Optimal conditions for the formation of this morphology of $Y_{2.5}Ce_{0.5}Fe_{2.5}Ga_{2.5}O_{12}$ nanopowder, such as short-term high-temperature combustion of a gel-like precursor with the release of a large amount of gaseous products, were provided by the PVA assisted gel combustion method. The results obtained in this work could be used in the future to develop efficient approaches to the synthesis of functional Ce-containing materials and to improve their properties.

Acknowledgements

References

[1] Garskaite E., Gibson K., et al. On the synthesis and characterization of iron-containing garnets ($Y_3Fe_5O_{12}$, YIG and $Fe_3Al_5O_{12}$, IAG). *Chemical Physics*, 2006, **323**, P. 204–210.

[2] McCloy J.S., Walsh B. Sublattice Magnetic Relaxation in Rare Earth Iron Garnets. *IEEE Transactions on Magnetics*, 2013, **49** (7), P. 4253–4256.

[3] Park M.B., Cho N.H. Structural and magnetic characteristics of yttrium iron garnet (YIG, Ce:YIG) films prepared by RF magnetron sputter techniques. *Journal of Magnetism and Magnetic Materials*, 2001, **231**, P. 253–264.

[4] Shen T., Dai H., Song M. Structure and Magnetic Properties of Ce-Substituted Yttrium Iron Garnet Prepared by Conventional Sintering Techniques. *Journal of Superconductivity and Novel Magnetism*, 2017, **30**, P. 937–941.

[5] Huang M., Zhang S. Growth and characterization of cerium-substituted yttrium iron garnet single crystals for magneto-optical applications. *Applied Physics A*, 2002, **74**, P. 177–180.

[6] Dastjerdi O.D., Shokrollahi H., Yang H. The enhancement of the Ce-solubility limit and saturation magnetization in the $Ce_{0.25}Bi_xPr_yY_{2.75-x-y}Fe_5O_{12}$ garnet synthesized by the conventional ceramic method. *Ceramics International*, 2020, **46** (315), P. 2709–2723.

[7] Ibrahim N.B., Edwards C., Palmer S.B. Pulsed laser ablation deposition of yttrium iron garnet and cerium-substituted YIG films. *Journal of Magnetism and Magnetic Materials*, 2000, **220**, P. 183–194.

[8] Xu H., Yang H. Magnetic properties of YIG doped with cerium and gadolinium ions. *Journal of Materials Science: Mater Electron*, 2008, **19**, P. 589–593.

[9] Shannon R.D. Revised effective ionic radii and systematic studies of interatomic distances in halides and chalcogenides. *Acta Crystallographica Section A*, 1976, **32**, P. 751–767.

[10] Gilleo M.A., Geller S. Magnetic and crystallographic properties of substituted yttrium-iron garnet, $3Y_2O_3 \cdot xM_2O_3 \cdot (5-x)Fe_2O_3$. *Physical Review*, 1958, **110** (1), P. 73–78.

[11] Bokshyts Y.V., Shevchenko G.P., et al. Structure and luminescence properties of $(Y_{1-x}La_x)_3(La_{1-y}Ga_y)O_{12}:Ce^{+3}$. *Inorganic Materials*, 2019, **55** (8), P. 820–826.

[12] Smirnova M.N., Nikiforova G.E., Goeva L.V. One-stage synthesis of $(Y_{0,5}Bi_{0.5})_3(Fe_{0.5}Ga_{0.5})_5O_{12}$ garnet using the organometallic gel auto-combustion approach. *Ceramics international*, 2018, **45** (4), P. 4509–4513.

[13] Smirnova M.N., Nipan G.D., Nikiforova G.E. $(Y_{1-x}Bi_x)_3(Fe_{1-y}Ga_y)_5O_{12}$ Solid Solution Region in the Ieneke Diagram. *Inorganic materials*, 2018, **54** (7), P. 683–688.

[14] Sharm V., Kuanr B.K. Magnetic and crystallographic properties of rare-earth substituted yttrium-iron garnet. *Journal of Alloys and Compounds*, 2018, **748**, P. 591–600.

[15] Opuchovic O., Andrulevicius M., et al. Cerium doping and cerium aluminium co-doping effects on the sol-gel processing of $Y_3Fe_5O_{12}$ (YIG): Bulk and thin films. *Solid State Sciences*, 2020, **99**, 106065.

[16] Kum J.S., Kim S.J., Shim I.B., Kim C.S. Magnetic properties of Ce-substituted yttrium iron garnet ferrite powders fabricated using a sol-gel method. *Journal of Magnetism and Magnetic Materials*, 2004, **272**, P. 2227–2229.

[17] Popova V.F., Petrosyan A.G., et al. Y_2O_3-Ga_2O_3 phase diagram. *Russian Journal of Inorganic Chemistry*, 2009, **54**, P. 624–629.

[18] Lomanova N.A., Tomkovich M.V., et al. Formation of $Bi_{1-x}Ca_xFeO_{3-\delta}$ Nanocrystals via Glycine-Nitrate Combustion. *Russian Journal of General Chemistry*, 2019, **89** (9), P. 1843–1850.

[19] Almjasheva O.V., Lomanova N.A., et al. The minimum size of oxide nanocrystals: phenomenological thermodynamic vs crystal-chemical approaches. *Nanosystems: Physics Chemistry Mathematics*, 2019, **10** (4), P. 428–437.

[20] Lisnevskaya I.V., Bobrova I.A., Lupeiko T.G. Synthesis of magnetic and multiferroic materials from polyvinyl alcohol-based gels. *Journal of Magnetism and Magnetic Materials*, 2016, **397**, P. 86–95.

[21] Zhuravlev V.D., Khaliullin S.M., Ermakova L.V., Bamburov V.G. Synthesis and Properties of Manganese Oxides Obtained via Combustion Reactions with Glycine and Citric Acid. *Russian Journal of Inorganic Chemistry*, 2020, **65**, P. 1522–1528.

[22] Nguyen A.T., Tran H.L.T., et al. Sol-gel synthesis and the investigation of the properties of nanocrystalline holmium orthoferrite. *Nanosystems: Physics Chemistry Mathematics*, 2020, **11** (6), P. 698–704.

[23] Matsnev M.E., Rusakov V.S. SpectrRelax: An Application for Mössbauer Spectra Modeling and Fitting. *AIP Conference Proceedings*, 2012, **1489**, P. 178–185.

[24] Nakatsuka A., Yoshiasa A., Takeno S. Site preference of cations and structural variation in $Y_3Fe_{5-x}Ga_xO_{12}$ ($0 \leq x \leq 5$) solid solutions with garnet structure. *Acta Crystallographica Section B*, 1995, **51**, P. 737–745.

[25] Sifat R., Beam J.C., Grosvenor A.P. Investigation of Factors That Affect the Oxidation State of Ce in the Garnet-Type Structure. *Inorganic Chemistry*, 2019, **58** (4), P. 2299–2306.

[26] Nicholson W.J., Bums G. Quadrupole Coupling Constant, eq/Qh, of Fe^{3+} in Several Rare-Earth Iron Garnets. *Physical Review A*, 1964, **133**, 1568.

[27] Sawatzky G.A., van der Woude F., Morrish A.H. Recoilless-Fraction ratios for Fe57 in octahe dral and tetrahedral sites of a spinel and a garnet. *Physical Review*, 1969, **183**, P. 383–386.

[28] Belogurov V.N., Bilinkin V.A. Dependence of the dynamic and hyperfine characteristics of Fe^{3+} ions on the rare-earth ion parameters in garnets above the Néel temperature. *Physica Status Solidi*, 1981, **63**, P. 45–53.